

Orientational bond and Néel order in the two-dimensional ionic Hubbard model

Mohsen Hafez-Torbati^{1,*} and Götz S. Uhrig^{1,†}

¹*Lehrstuhl für Theoretische Physik I, Technische Universität Dortmund,
Otto-Hahn-Straße 4, 44221 Dortmund, Germany*

(Dated: May 19, 2016)

Unconventional phases often occur where two competing mechanisms compensate. An excellent example is the ionic Hubbard model where the alternating local potential δ , favoring a band insulator (BI), competes with the local repulsion U , favoring a Mott insulator (MI). By continuous unitary transformations we derive effective models in which we study the softening of various excitons. The softening signals the instability towards new phases that we describe on the mean-field level. On increasing U from the BI in two dimensions, we find a bond-ordered phase breaking orientational symmetry due to a d-wave component. Then, antiferromagnetic order appears coexisting with the d-wave bond order. Finally, the d-wave order vanishes and a Néel-type MI persists.

PACS numbers: 71.30.+h, 71.10.Li, 71.10.Fd, 74.20.Fg

Searching for unconventional states of matter and non-trivial elementary excitations (quasiparticles (QPs)) is one of the crucial objectives of the research in strongly correlated lattice models. Outstanding examples range from the quasi long-range ordered Mott insulator (MI) in one dimension (1D) where the neutral spin-1/2 particle “spinon” represents the elementary excitation to quantum spin ice in three dimensions (3D) where magnetic monopoles represent the QPs. In order to find unexpected phases, it is a good idea to focus on parameter regions where two antagonists compensate because then subtle subleading mechanisms can take over.

The present article addresses the IHM in two dimensions (2D) on the square lattice in order to understand which phases possibly arise between the band insulator (BI) and the MI. Its Hamiltonian reads

$$H = \frac{\delta}{2} \sum_{\mathbf{r},\sigma} (-1)^{i+j} n_{\mathbf{r},\sigma} + U \sum_{\mathbf{r}} (n_{\mathbf{r},\uparrow} - \frac{1}{2})(n_{\mathbf{r},\downarrow} - \frac{1}{2}) + t \sum_{\langle \mathbf{r}\mathbf{r}' \rangle, \sigma} (c_{\mathbf{r},\sigma}^\dagger c_{\mathbf{r}',\sigma} + \text{h.c.}), \quad (1)$$

where $\mathbf{r} := i\hat{x} + j\hat{y}$ spans the square lattice, $c_{\mathbf{r},\sigma}^\dagger$ ($c_{\mathbf{r},\sigma}$) is the fermionic creation (annihilation) operator at site \mathbf{r} with spin σ , and $n_{\mathbf{r},\sigma} := c_{\mathbf{r},\sigma}^\dagger c_{\mathbf{r},\sigma}$ is the occupation operator. The sum over $\langle \mathbf{r}\mathbf{r}' \rangle$ restricts the hopping to nearest-neighbor sites. Initially, the IHM was introduced to describe the neutral-ionic transition in mixed-stack organic compounds¹ and was later used for the description of ferroelectric perovskites².

In 1D, it is well understood that the BI at small Hubbard interaction U is separated from quasi-long-range ordered MI at large U by an intermediate phase with alternating bond order (BO)³. The position of the two transition points (U_{c1} from BI to BO and U_{c2} from BO to MI)^{4,5} and the excitation spectrum^{6,7} of the model are determined quantitatively. We highlight that the transition to the BO phase is signaled by the softening of an exciton³⁻⁵ located at momentum π (setting the lattice constant to unity)^{6,7}.

In 2D, the limiting BI and MI phases are expected at low and high U , respectively. The MI at large U shows long-range antiferromagnetic order of Néel type (AF)⁸. But existence and properties of intermediate phases is highly controversial. A determinant quantum Monte Carlo (DQMC) analysis of small clusters identifies an intermediate metallic region without magnetic or bond order⁹. Cluster dynamic mean-field theory (DMFT) indicates an intermediate phase with an incommensurate bond order and a finite staggered magnetization¹⁰. Single-site DMFT of the half-filled IHM on the Bethe lattice suggests a single transition point separating the BI from the magnetically ordered MI.¹¹

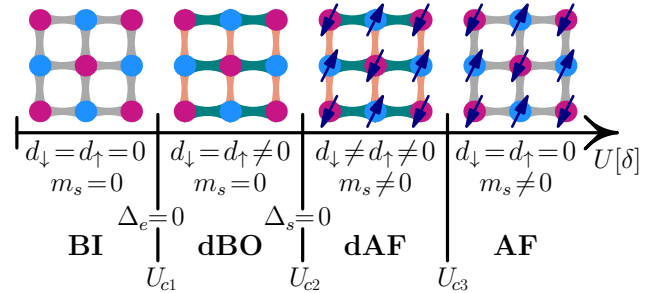


Figure 1. (color online) Scheme of the phase transitions in the 2D IHM. The staggered magnetization is denoted by m_s and the spin-dependent d-wave bond order parameter by d_σ . The $S = 0$ exciton gap is Δ_e and Δ_s is the spin gap (or $S = 1$ exciton)⁶.

We study the 2D IHM by continuous unitary transformations (CUTs)¹² realized in real space up to higher orders in the hopping t . The flow equations are closed using the directly evaluated enhanced perturbative CUT (deepCUT)¹³. In this way, an effective model is derived in terms of the elementary fermionic QPs. The virtual processes are eliminated as in the derivation of a t - J model from a Hubbard model¹⁴⁻¹⁷. The effective model allows us to address the interaction of two of these QPs. A particle and a hole attract each other and may form a bound state, an exciton. The softening of such

excitons indicate the instability of the phase towards a condensation of these excitons. In this fashion, we determined the BI-to-BO transition value U_{c1} of the 1D IHM within 0.3%⁶. We stress that already the second order calculation in the hopping t yields qualitatively the correct result, i.e., the correct symmetries for the condensate phase, in spite of the very small energy scales t^2/U (relative to δ) driving the transition^{6,7}. Thus we adopt the same strategy in 2D where the CUT has been successfully used before^{18,19}, in particular for binding phenomena²⁰.

We are using the double 1-particle gap $\Delta_c := 2(E_0^{N+1} - E_0^N)$, the singlet exciton gap $\Delta_e := E_{1,S=0}^N - E_0^N$, and the spin (triplet) exciton gap $\Delta_s := E_{1,S=1}^N - E_0^N$ where E_0^N stands for the ground state energy and $E_{1,S}^N$ for the first excited state with total spin S for N electrons. At half-filling, the number of electron N equals the number of lattice sites. In the absence of any electron-electron bound state, Δ_c , being twice the minimum of the fermion dispersion, equals the charge gap. We use the term charge gap because it has been used in previous papers on the IHM⁴⁻⁷.

Fig. 1 summarizes our key results: Upon increasing U in the BI, the exciton gap Δ_e reduces till it vanishes at U_{c1} where d-wave bond order (dBO) sets in. In this phase, the 90° rotation symmetry of the square lattice is broken and the d-wave bond order parameter d_σ becomes finite. Then, the spin gap Δ_s closes at U_{c2} beyond which the staggered Néel magnetization m_s becomes finite and the d-wave order parameter d_σ starts depending on spin (dAF). Eventually, the rotational symmetry is restored at U_{c3} ($d_\sigma = 0$) while the Néel order persists (AF).

Technically, we proceed as in 1D⁶ by transforming the half-filled IHM into a translationally invariant problem. On the odd sublattice ($i + j$ odd), we apply the electron-hole transformation $T^{(eh)}$: $c_{\mathbf{r},\sigma}^\dagger \rightarrow h_{\mathbf{r},\sigma}$. For consistency, we then use for particle and hole creation the same operator $f_{\mathbf{r},\sigma}^{(\dagger)}$. The local phase transformation $T^{(l)}$: $f_{\mathbf{r},\sigma}^\dagger \rightarrow e^{i\frac{\pi}{2}(x+y)} e^{-i\frac{\pi}{4}} f_{\mathbf{r},\sigma}^\dagger$ yields

$$H = (U - 2\delta)/4 \sum_{\mathbf{r}} \mathbb{1} + t \sum_{\langle \mathbf{r}\mathbf{r}' \rangle, \sigma} (f_{\mathbf{r},\sigma}^\dagger f_{\mathbf{r}',\sigma}^\dagger + \text{h.c.}) + (\delta - U)/2 \sum_{\mathbf{r},\sigma} f_{\mathbf{r},\sigma}^\dagger f_{\mathbf{r},\sigma} + U \sum_{\mathbf{r}} f_{\mathbf{r},\uparrow}^\dagger f_{\mathbf{r},\downarrow}^\dagger f_{\mathbf{r},\downarrow} f_{\mathbf{r},\uparrow}. \quad (2)$$

The phase transformation $T^{(l)}$ induces a shift in momentum space by $\pi/2 := (\pi/2, \pi/2)$ for single f -fermions. The electron-hole transformation $T^{(eh)}$ modifies the spin and the charge on the odd sublattice according to

$$(S_{\mathbf{r}}^x, S_{\mathbf{r}}^y, S_{\mathbf{r}}^z, n_{\mathbf{r},\sigma}) \longrightarrow (-S_{\mathbf{r}}^x, +S_{\mathbf{r}}^y, -S_{\mathbf{r}}^z, 1 - n_{\mathbf{r},\sigma}). \quad (3)$$

Hence, the AF phase in the original c -fermions appears as translationally invariant ferromagnet in the f -fermions. The staggered magnetization reads $m_s := \frac{1}{2} \sum_{\sigma} \text{sgn}(\sigma) \langle f_{\mathbf{0},\sigma}^\dagger f_{\mathbf{0},\sigma} \rangle$. The d-wave order parameter reads $d_\sigma := \langle f_{\mathbf{0},\sigma}^\dagger f_{\hat{x},\sigma}^\dagger \rangle - \langle f_{\mathbf{0},\sigma}^\dagger f_{\hat{y},\sigma}^\dagger \rangle$.

We apply the deepCUT to (2) eliminating processes which let single f -fermions and pairs of them decay. We

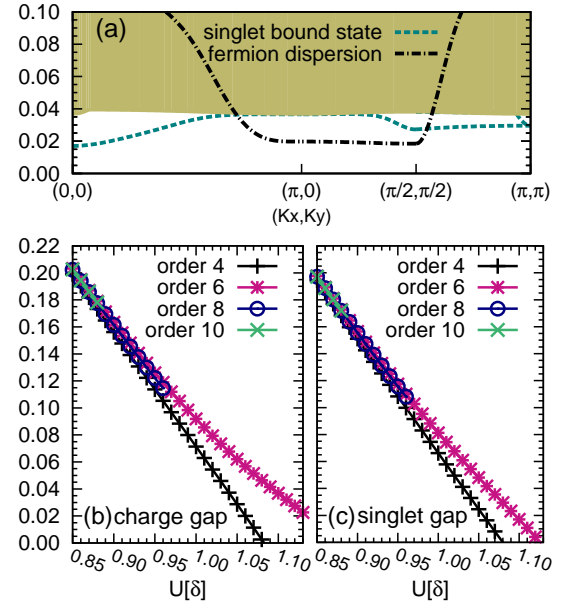


Figure 2. (color online) (a) Low-energy excitations for $t = 0.05\delta$ and $U = 1.1\delta$ in order 6; charge gap Δ_c (b) and singlet gap Δ_s (c) in units of δ versus U .

disentangle the one-QP and the two-QP subspaces from the remaining Hilbert space by a suitable change of basis such that the 1-QP dispersion and the dispersion of bound states such as excitons become accessible. Technically, we employ the reduced generator $n : 2^{21}$ targeting the 0-, 1-, and 2-QP sector¹³. The sign of the terms in the generator, i.e., the sense of rotation, is chosen first according to the change in the number of double occupancy (increase of double occupancy leads to the same sign in the generator as in the Hamiltonian). If this number is not changed, the change in the number of fermions determines the sign. In this way, we map the Hamiltonian (2) to the effective Hamiltonian

$$H_{\text{eff}} = E_0 + \sum_{\mathbf{r},\sigma} \sum_{\mathbf{d}} \sigma [C_1^1]^d (f_{\mathbf{r},\sigma}^\dagger f_{\mathbf{r}+\mathbf{d},\sigma}^\dagger + \text{h.c.}) + H_2^2 \quad (4)$$

where H_2^2 stands for interaction terms of two creation and two annihilation operators with coefficients C_2^2 . The effective coefficients C_1^1 and C_2^2 are determined from the flow equation $\partial_\ell H = [\eta, H]$ ^{12,13,21-23}. Higher particle interactions are ignored. The range of processes in (4) is limited by the order in t of the deepCUT. The calculations are restricted to order 6 because for higher orders overlapping continua prevent a well-defined convergence of the flow²¹. Thus the effective Hamiltonian is not fully quantitative, but it is qualitatively correct. For an assessment of the accuracy see Refs. 6 and 7; technical aspects related to simplification rules are given in Appendix A.

The effective Hamiltonian (4) allows us to determine the ground state energy, the 1-QP dispersion, and bound pairs of 2 QPs. Due to the particle-hole transformation $T^{(eh)}$ excitons with odd distance between their con-

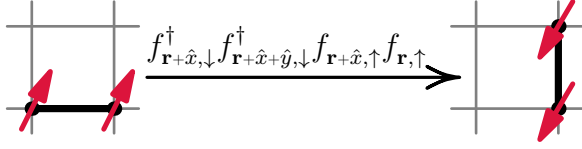


Figure 3. Correlated hopping $f_{\mathbf{r}+\hat{x},\downarrow}^\dagger f_{\mathbf{r}+\hat{x}+\hat{y},\downarrow}^\dagger f_{\mathbf{r}+\hat{x},\uparrow} f_{\mathbf{r},\uparrow}$. Recall that the spin configuration shown is a particle-hole singlet in the original c -fermions.

stituents appear in the effective model as pairs of particles. The eigenvalues in the 2-QP subspace are found for fixed total momentum \mathbf{k} , total spin S , and total S^z component M as in the 1D case⁶. Fig. 2(a) depicts the low-energy spectrum in the BI phase consisting of the fermionic dispersion and a singlet exciton; no triplet exciton is found. Note the rather flat dispersion and lower continuum edge.

Very interestingly, the singlet exciton takes its minimum at $\mathbf{k} = (0,0)$. In 1D, its minimum was at $k = \pi$ so that its condensation led to *dimerized* bond order^{3,6}. The fact that the singlet exciton softens at a different momentum clearly shows that the condensed phase beyond the BI will no longer be a dimerized BO. Figs. 2(b) and (c) display the charge and the singlet gap vs. U . Generally, the softening of a bosonic excitation implies the divergence of the susceptibility with the same symmetries $\chi(\omega)$ at $\omega = 0$ because $\chi(\omega)$ corresponds to the bosonic propagator up to matrix elements. Thus it has a pole at the boson eigen energy moving to $\omega = 0$ upon softening. The direct access to the energies of bound states avoids the necessity to guess the correct symmetry of the diverging susceptibility. In order 4, the singlet gap Δ_e vanishes at $U_{c1} = 1.08\delta$ where the charge gap Δ_c is still finite at 0.003δ . In order 6, we find $U_{c1} = 1.126\delta$ with $\Delta_c = 0.023\delta$. Considering all available orders and comparing to the 1D results⁶, we estimate that the transition point U_{c1} lies between $U = 1.08\delta$ and $U = 1.126\delta$. The value of the charge gap at the transition point is also expected to be between the results in order 4 and order 6, similar to 1D findings⁷. Increasing t to 0.1δ the transition point shifts to larger values of U , see Appendix B.

The key observation is that the $S = 0$ exciton softens *before* the system would become metallic in analogy to the 1D case, but with *other* symmetries. The exciton condensation leads to a phase without magnetic order because the condensing exciton has no spin. The condensation does not break translational invariance because the exciton condenses at zero total momentum. The analysis of the point group properties of the exciton reveals that its wave function becomes negative upon spatial rotation by 90° so that the condensed phase should display the same d-wave symmetry.

The mechanism for electron and hole to form a bound state with d-wave symmetry relies on the interaction $f_{\mathbf{r}+\hat{x},\downarrow}^\dagger f_{\mathbf{r}+\hat{x}+\hat{y},\downarrow}^\dagger f_{\mathbf{r}+\hat{x},\uparrow} f_{\mathbf{r},\uparrow}$ representing correlated hop-

ping, see Fig. 3. Such terms, occurring already in the second order in t with positive sign, have a singlet on a bond in \hat{x} -direction hop to a bond in \hat{y} -direction²⁴. This correlated hopping corresponds to the well-known three-site terms in the t - J model^{14–17}. If the wave function has the opposite sign on \hat{y} -bonds of those on \hat{x} -bonds this correlated hopping leads to attraction and eventually to a bound state with d-wave symmetry.

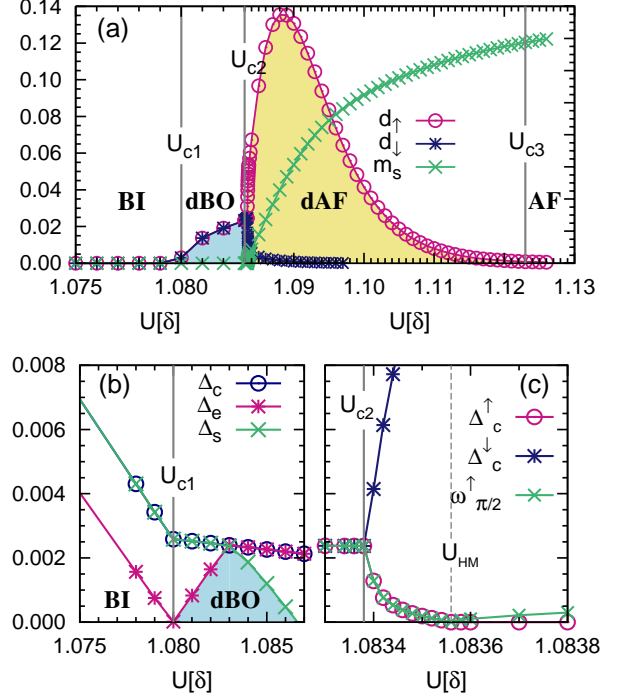


Figure 4. (color online) Staggered magnetization density m_s and d-wave bond order parameter d_σ (panel (a)) and charge gap Δ_c^σ , singlet gap Δ_e , and spin gap Δ_s (panels (b) and (c)) in units of δ versus U for $t = 0.05\delta$ at order 4.

Similar to the 1D case⁶, we describe this condensed phase by a self-consistent BCS-type MF theory applied to (4), see Fig. 4(a) to the left of U_{c2} . This approach is exact for $U \leq U_{c1}$ where the quantum fluctuations are already considered by the CUT. In particular, the onset of order occurs precisely where the exciton energy vanishes as required by consistency. For $U > U_{c1}$ the MF approach is a good approximation systematically controlled by the distance $U > U_{c1}$. The order of the calculations is 4 in powers of t and $t = 0.05\delta$. Its bond order d_σ consists in the difference of the bonds in x and in y direction implying d-wave character. We determine the expectation values $\langle f_{0,\sigma}^\dagger f_{\mathbf{d},\sigma} \rangle$ and $\langle f_{0,\sigma}^\dagger f_{\mathbf{d},\sigma}^\dagger \rangle$ self-consistently, see Appendix C, comprising also the magnetization m_s and the d-wave order parameter d_σ .

The singlet and the triplet excitons *within* the dBO are determined by analysing the 2-QP problem neglecting the off-diagonal terms linking 2-QP states to states of higher particle number, see Appendix C for the details. This leads to the gaps displayed in Fig. 4(b). The

exciton gap Δ_e quickly increases till the exciton ceases to exist because it merges with the 2-QP continuum. In parallel, a triplet exciton is formed and softens. The results of order 6, given in Appendix D, are qualitatively similar. Hence the system becomes unstable towards the condensation of a magnetic bosons, i.e., towards magnetic ordering. The softening occurs at momentum π in the original model so that this triplon condensation is the expected Néel ordering.

We study the Néel ordering by allowing for spin dependent MF solutions of (4), i.e., m_s becomes finite and $d_\uparrow \neq d_\downarrow$. In addition, the charge gap becomes also spin dependent $\Delta_c^\uparrow \neq \Delta_c^\downarrow$. We find that the d-wave order does not vanish, but that it persists so that antiferromagnetism and d-wave order coexist and a d-wave antiferromagnet (dAF) forms. This solution occurs at and beyond $U_{c2} \approx 1.083\delta$ as shown in Fig. 4(a) and in the zoom (c).²⁵

So far, we constructed the phase diagram following the spontaneous symmetry breaking indicated by soft excitons. In the dAF phase, the symmetry is strongly reduced. For large U , however, we expect Néel ordering without d-wave components because the Hubbard model maps to the Heisenberg model since the ionic alternation is only a small perturbation for $U \gg \delta$. The MF solution retrieves this feature. The BO parameters d_σ quickly decrease on increasing U . For $U > 1.123\delta$, d_\uparrow is smaller than 10^{-3} . We conclude that there is a U_{c3} beyond which the spatial rotation is restored as a symmetry of the IHM: the dAF phase becomes a Néel ordered AF phase. The precise value of U_{c3} is difficult to pinpoint because $d_\uparrow(U)$ is consistent with an exponential decrease $\propto \exp(C/(U - U_{c3}))$ with $U_{c3} \approx 1.24\delta$. This resembles a Kosterlitz-Thouless type of transition as also proposed in Ref. 10. But the numerics is too involved and the energy scales too small to identify the decrease of $d_\uparrow(U)$ unambiguously.

In Fig. 4(c), we also plot the spin-dependent charge gaps in the vicinity of U_{c2} . Beyond U_{c2} , Δ_c^\downarrow increases quickly, but Δ_c^\uparrow decreases and hits zero at a half-metallic point U_{HM} . Such half-metallic points occurred in previous analyses already¹¹. The spin-up charge gap is located at momentum $\mathbf{k} = \pi/2$ up to U_{HM} , but for $U > U_{HM}$ it moves to incommensurate momenta at the line $k_x = k_y$ and remains zero. But we cannot exclude that the zero Δ_c^\uparrow for $U > U_{HM}$ is an artefact of our approach. Any small deviation from the particle-conserving effective Hamiltonian (4) would spoil this feature. Thus we also included $\omega_{\pi/2}^\uparrow$ in Fig. 4(c) displaying a more generic behavior.

Summarizing, we studied unconventional phases in the ionic Hubbard model in 2D between the known band insulator at weak interaction and the Néel ordered Mott insulator at strong interaction. We found bond order which spontaneously breaks the orientational symmetry: d-wave bond order (dBO). Even a region of coexistence of bond order and Néel order is identified: d-wave bond order and antiferromagnetism (dAF). Thereby, we provide

clarification for the so far ambiguous evidence concerning the influence of strong interactions on band insulators. We stress that no weak-coupling instabilities indicate the existence of these phases. This underlines that these phases are inherent to strong coupling²⁶. Against this background, we think that the single-site DMFT¹¹ does not capture the spatial correlations indispensable for d-wave ordering and the DQMC⁹ considers too small clusters at too large temperatures to capture the small energy scales driving the transitions found. The cluster DMFT¹⁰ also advocated bond order, but combined with dimerization and incommensurability. Since the rotational symmetry was not allowed to be broken no d-wave ordering could be detected.

We emphasize that the scenario discovered here is different from the bond ordered phases with d-wave symmetry discussed in the literature so far. These previous scenarios imply either a kind of alternation^{26,27} or incommensurability^{28,29} and they usually occur *away* from half-filling in contrast to our finding. The dBO phase presently advocated induces no dimerization and breaks only the rotational symmetry of the square lattice.

The conclusions are based on effective models expressed in elementary excitations. This approach was successful in 1D. No *ad hoc* assumptions about broken symmetries are made, but instabilities are systematically deduced from softening bound states, namely singlet and triplet excitons, the latter being the spin excitations. The quantum numbers and symmetries of the excitonic wave function implies the symmetry of the phase to which the instable phase evolves. In this way, two continuous phase transitions at U_{c1} and U_{c2} are identified. Based on symmetry considerations, we expect the first transition to be in the Ising and the second transition to be in the $O(3)$ universality class.

We consider the obtained scenario to be complete because the d-wave order quickly decreases in the dAF phase so that only Néel order remains beyond a third transition interaction U_{c3} as expected for large interaction U .

The findings indicate for which types of correlations one has to look in order to identify intermediate phases in the wide research field between band insulating and Mott insulating phases, for instance on various lattices.

ACKNOWLEDGMENTS

We are grateful to the Helmholtz Virtual Institute “New states of matter and their excitations” for financial support.

Appendix A: Simplification Rules

Here we present the simplification rules used to realize the comprehensive CUTs, cf. Ref. 13.

The basic *a-posteriori* and *a-priori* simplification rules (SRs) introduced in Ref. 6 can be used for the IHM on the square lattice because they are lattice independent. In addition, we have implemented an extended *a-posteriori* SR. The aim is to estimate whether a monomial A contributes to the targeted quantities up to a specific order, for example n , or not. We explain the extended *a-posteriori* SR for the creation operators in A . The annihilation part can be analyzed in the same way.

Similar to the 1D case, one can treat spin-up and spin-down operators separately⁶. From the position of creation operators with spin σ , we form a cluster (graph). We consider a vertex for each lattice site and add an edge between two vertices if the corresponding sites are adjacent. The degree of a vertex is defined as the number of edges linked to the vertex. The cluster is divided into a set of linked subclusters. Let us consider one of the subclusters and denote it by \mathcal{C} . In the first step, we need to underestimate the number of commutations $K[\mathcal{C}]$ necessary to cancel the arbitrary linked cluster \mathcal{C} .

The size of \mathcal{C} is reduced in an *iterative* way. We eliminate each vertex with degree 1 and the vertex it is linked to. This costs one commutation for each of these pairs to be omitted. Let us suppose that after $p_{\mathcal{C}}$ commutations no vertex with degree 1 is left. This reduces the linked cluster \mathcal{C} to isolated vertices and/or to the linked subclusters \mathcal{C}' which has no vertex with degree 1. Each isolated vertex requires one commutation to be canceled. We denote by $s_{\mathcal{C}}$ the number of isolated vertices. One also needs $\left\lceil \frac{v_{\mathcal{C}'}}{2} \right\rceil$ commutations to cancel the subcluster \mathcal{C}' which has $v_{\mathcal{C}'}$ vertices. $\lceil x \rceil$ is defined as smallest integer not less than x . Hence, we obtain

$$K[\mathcal{C}] \geq \tilde{K}[\mathcal{C}] := p_{\mathcal{C}} + s_{\mathcal{C}} + \sum_{\mathcal{C}'} \left\lceil \frac{v_{\mathcal{C}'}}{2} \right\rceil \quad (\text{A1a})$$

$$\geq p_{\mathcal{C}} + s_{\mathcal{C}} + \left\lceil \frac{v_{\mathcal{C}}^r}{2} \right\rceil, \quad (\text{A1b})$$

where $v_{\mathcal{C}}^r := \sum_{\mathcal{C}'} v_{\mathcal{C}'}$. One can use the simpler Eq. (A1b) instead of (A1a) for $\tilde{K}[\mathcal{C}]$. There should be at least two subclusters \mathcal{C}' each one with an odd number of vertices to change the “equal” sign in (A1b) into “greater than”. For the square lattice, this means that the initial linked cluster \mathcal{CF} should contain at least 16 ($=7+7+2$) vertices.

One can check that Eq. (A1) simplifies to the 1D counterpart where no subcluster \mathcal{C}' can exist⁶. As example, let us examine the three clusters in Fig. 5. We find $p_{\mathcal{C}} = 1$, $s_{\mathcal{C}} = 2$, and no \mathcal{C}' for Fig. 5(a), $p_{\mathcal{C}} = 2$, $s_{\mathcal{C}} = 2$, and no \mathcal{C}' for Fig. 5(b), and finally $p_{\mathcal{C}} = 1$, $s_{\mathcal{C}} = 0$, and one subcluster \mathcal{C}' with $v_{\mathcal{C}'} = 4$ for Fig. 5(c).

The total number of commutations \tilde{K}_0^c required to cancel all the creation operators of A is given by

$$\tilde{K}_0^c := \sum_{\mathcal{C}} \tilde{K}[\mathcal{C}] \quad (\text{A2})$$

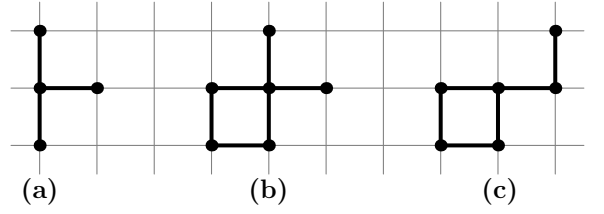


Figure 5. Three kinds of linked clusters on the square lattice.

where the sum runs over all linked spin-up and spin-down clusters of monomial A . Similar to the rules presented in Ref. 13, Eq. (A2) can be extended to \tilde{K}_q^c where sectors up to q quasiparticles are targeted. The aim is to keep q operators such that the maximal order of A is overestimated¹³. We first keep the operators which can save one commutation. The total number of these operators is given by

$$d := \sum_{\mathcal{C}} d_{\mathcal{C}} := \sum_{\mathcal{C}} (s_{\mathcal{C}} + v_{\mathcal{C}}^r \bmod 2), \quad (\text{A3})$$

where we suppose that (A1b) holds for $\tilde{K}[\mathcal{C}]$. The remaining operators (if $q > d$) can save one commutation per pair. Therefore, we find

$$\tilde{K}_q^c = \max \left(\tilde{K}_0^c - \left\lfloor \frac{q + d'}{2} \right\rfloor, 0 \right), \quad (\text{A4})$$

where $d' := \min(d, q)$. In the same way, one can analyze the annihilation part of the monomial A to find \tilde{K}_q^a . The monomial A can be discarded if

$$O_{\min}(A) > n - \tilde{K}_q^c - \tilde{K}_q^a, \quad (\text{A5})$$

where $O_{\min}(A)$ is the minimal order of A ¹³.

Appendix B: Results for Larger Hopping

In order to show that the results obtained in the main text also apply for larger values of the hopping. Fig. 6(a) represents the same quantities as Fig. 2(a) but for $t = 0.1\delta$ and $U = 1.25\delta$. Figs. 6(b) and (c) are the same as Figs. 2(b) and (c), but for $t = 0.1\delta$. One can see that by increasing t from $t = 0.05\delta$ to $t = 0.1\delta$, the position of the first transition point is shifted to the larger values of U . The value of the charge gap at the transition point is also increased compared to the case for $t = 0.05\delta$. This behaviour is similar to what is found for the 1D IHM by DMRG⁴. Larger hopping increases the energy scale on which the relevant physics takes place in the ionic Hubbard model (IHM).

Appendix C: BCS-Type Mean-Field Analysis

The Hamiltonian (4) is normal-ordered with respect to the bilinear part using Wick's theorem. The bilin-

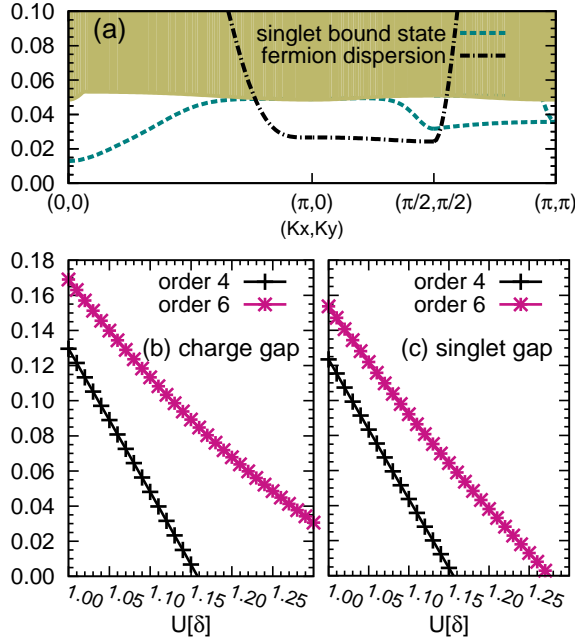


Figure 6. (a) The same as Fig. 2(a) in the main text, but for $t = 0.1\delta$ and $U = 1.25\delta$. (b) and (c) are also the same as Fig. 2(b) and (c) in the main text, but for $t = 0.1\delta$.

ear Hamiltonian is diagonalized in momentum space by a Bogoliubov transformation. The relevant expectation values are given by

$$\langle f_{0,\sigma}^\dagger f_{d,\sigma} \rangle = \frac{\delta_{d,0}}{2} - \frac{1}{2\pi^2} \int_{(-\frac{\pi}{2},0)}^{(\frac{\pi}{2},\pi)} \frac{\tilde{c}_{\mathbf{k}}^\sigma}{\omega_{\mathbf{k}}^\sigma} \cos(\mathbf{k} \cdot \mathbf{d}) d\mathbf{k}, \quad (\text{C1a})$$

$$\langle f_{0,\sigma}^\dagger f_{d,\sigma}^\dagger \rangle = -\frac{1}{2\pi^2} \int_{(-\frac{\pi}{2},0)}^{(\frac{\pi}{2},\pi)} \frac{\tilde{\Gamma}_{\mathbf{k}}^\sigma}{\omega_{\mathbf{k}}^\sigma} \sin(\mathbf{k} \cdot \mathbf{d}) d\mathbf{k}, \quad (\text{C1b})$$

where $\tilde{c}_{\mathbf{k}}^\sigma := c_0^\sigma + 2 \sum_{\mathbf{d}} c_{\mathbf{d}}^\sigma \cos(\mathbf{k} \cdot \mathbf{d})$, $\tilde{\Gamma}_{\mathbf{k}}^\sigma := 2 \sum_{\mathbf{d}} \Gamma_{\mathbf{d}}^\sigma \sin(\mathbf{k} \cdot \mathbf{d})$,

and $\omega_{\mathbf{k}}^\sigma := \sqrt{\tilde{c}_{\mathbf{k}}^{\sigma^2} + \tilde{\Gamma}_{\mathbf{k}}^{\sigma^2}}$.

The coefficients $c_{\mathbf{d}}^\sigma$ and $\Gamma_{\mathbf{d}}^\sigma$ are defined as prefactors of normal-ordered hopping and Bogoliubov operators over the distance \mathbf{d} , respectively. Conservation of total charge guarantees that no hopping term over odd and no Bogoliubov term over even distances occurs. One can omit the spin indices from Eqs. (C1) because the SU(2) symmetry is preserved in the d-wave bond order (dBO) phase. The general spin-dependent form helps us to analyze also phases with broken spin symmetry. After some standard calculations, the Hamiltonian (4) be rewritten as

$$H_{\text{eff}} = \tilde{E}_0 \mathbb{1} + \sum_{\mathbf{k},\sigma} \omega_{\mathbf{k}} \lambda_{\mathbf{k},\sigma}^\dagger \lambda_{\mathbf{k},\sigma} + \sum_{\mathbf{k},\mathbf{q};\mathbf{q}_f} \sum_{\substack{\sigma_1,\sigma_2 \\ \beta_1,\beta_2}} \frac{\beta_2\beta_1}{\sigma_2\sigma_1} [\tilde{C}_2^2]_{\mathbf{q}_i}^{\mathbf{k}\mathbf{q}_f} \lambda_{\mathbf{k}/2+\mathbf{q}_f,\beta_2}^\dagger \lambda_{\mathbf{k}/2-\mathbf{q}_f,\beta_1}^\dagger \lambda_{\mathbf{k}/2+\mathbf{q}_i,\sigma_2} \lambda_{\mathbf{k}/2-\mathbf{q}_i,\sigma_1} + \dots, \quad (\text{C2})$$

where the operator $\lambda_{\mathbf{k},\sigma}^{(\dagger)}$ is defined such that it diagonalizes the non-interacting part of the Hamiltonian. The coefficients of the interaction potential in momentum space \tilde{C}_2^2 are given in terms of the real space interactions C_2^2 and the hopping coefficients $\tilde{c}_{\mathbf{k}}$ and the Bogoliubov coefficients $\tilde{\Gamma}_{\mathbf{k}}$. The “...” stand for the quartic off-diagonal interactions $\tilde{H}_1^3 \propto \lambda^\dagger \lambda^\dagger \lambda^\dagger \lambda$ and $\tilde{H}_0^4 \propto \lambda^\dagger \lambda^\dagger \lambda^\dagger \lambda^\dagger$ and their hermitian conjugates.

Taking the ground-state energy of the mean-field approximation as the true ground-state energy neglects the terms $\tilde{H}_0^4 + \tilde{H}_4^0$. They are systematically controlled by $U - U_{c1}$, i.e., they are indeed small in the parameter regime considered.

Considering the 1-particle dispersion $\omega_{\mathbf{k}}$ in Eq. (C2) and/or the interactions in the 2-particle sector above the mean-field solution, we also neglect the terms $\tilde{H}_1^3 + \tilde{H}_3^1$ which are again systematically controlled by $U - U_{c1}$. The singlet and the triplet 2-particle bound states in Fig. 4(b) of the main text are determined by exact diagonalization in the 2-particle subspace for fixed total momentum \mathbf{k} , total spin S , and total magnetic number M . The remaining quantum number is the relative momentum \mathbf{q} which is not conserved.

There is, however, a subtle point to be noticed. In

the 2-particle state $|\mathbf{k}; \mathbf{q}\rangle_{\sigma_1\sigma_2} := \lambda_{\mathbf{k}/2+\mathbf{q},\sigma_1}^\dagger \lambda_{\mathbf{k}/2-\mathbf{q},\sigma_2}^\dagger |0\rangle$, states with two electrons (two holes) and one electron and one hole are mixed. In order to stay in the half-filled case, we define $|\mathbf{k}; \mathbf{q}\rangle_{\sigma_1\sigma_2}^{Q=0} := \frac{1}{\sqrt{2}}(|\mathbf{k}; \mathbf{q}\rangle_{\sigma_1\sigma_2} + |\mathbf{k}; \pi-\mathbf{q}\rangle_{\sigma_2\sigma_1})$ which has the net total charge $Q = 0$. The relative momentum \mathbf{q} is now restricted, e.g., to $0 < q_x < \pi$ and $-\frac{\pi}{2} < q_y < \frac{\pi}{2}$. We employ triplet states ($S = 1$) with specific polarizations rather than specific magnetic numbers. The triplet states are given by $|t_x\rangle = \frac{1}{\sqrt{2}}(|\uparrow\downarrow\rangle + |\downarrow\uparrow\rangle)$, $|t_y\rangle = \frac{-i}{\sqrt{2}}(|\uparrow\downarrow\rangle - |\downarrow\uparrow\rangle)$, $|t_z\rangle = \frac{1}{\sqrt{2}}(|\uparrow\uparrow\rangle - |\downarrow\downarrow\rangle)$, and the singlet state by $|s\rangle = \frac{1}{\sqrt{2}}(|\uparrow\uparrow\rangle + |\downarrow\downarrow\rangle)$.

Constructing the Hamiltonian matrix in momentum space is time consuming compared to the real space diagonalization. This is the case because for each \mathbf{q}_i and \mathbf{q}_f in (C2), one has to perform three summations over weighted real space interaction coefficients to calculate $\sum_{\beta_2\beta_1} \sum_{\sigma_2\sigma_1} [\tilde{C}_2^2]_{\mathbf{q}_i}^{\mathbf{k}\mathbf{q}_f}$.

Appendix D: Results in Order t^6

In order to underline that the analysis in the main text is supported by results in higher order of the hop-

ping. Figs. 7(a) and (b) represent the same quantities as Fig. 4(a) for $U < U_{c2}$ and Fig. 4(b), but in order 6. Divergence of the flow equations prevents us to consider interactions beyond $U = 1.155\delta$, so that we can not access the full phase diagram.

REFERENCES

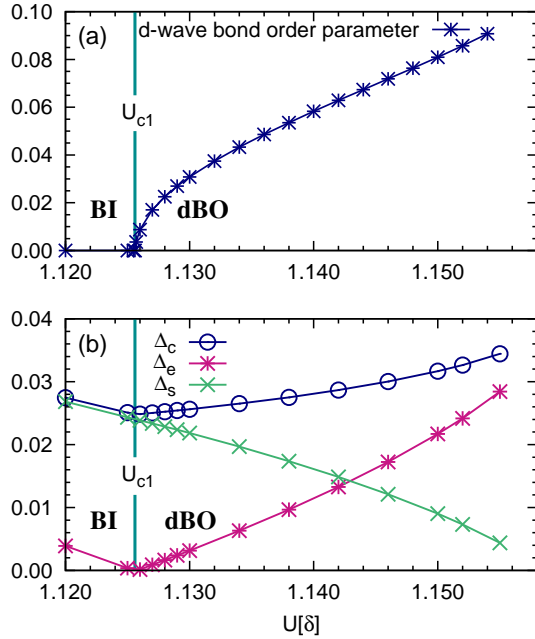


Figure 7. The same as in Fig. 4(a) for $U < U_{c2}$ and Fig. 4(b), but in order 6 of the hopping.

* mohsen.hafez@tu-dortmund.de

† goetz.uhrig@tu-dortmund.de

- ¹ N. Nagaosa and J. Takimoto, *Journal of the Physical Society of Japan* **55**, 2735 (1986).
- ² T. Egami, S. Ishihara, and M. Tachiki, *Science* **261**, 1307 (1993).
- ³ M. Fabrizio, A. O. Gogolin, and A. A. Nersesyan, *Phys. Rev. Lett.* **83**, 2014 (1999).
- ⁴ S. R. Manmana, V. Meden, R. M. Noack, and K. Schönhammer, *Phys. Rev. B* **70**, 155115 (2004).
- ⁵ L. Tincani, R. M. Noack, and D. Baeriswyl, *Phys. Rev. B* **79**, 165109 (2009).
- ⁶ M. Hafez Torbati, N. A. Drescher, and G. S. Uhrig, *Phys. Rev. B* **89**, 245126 (2014).
- ⁷ M. Hafez-Torbati, N. A. Drescher, and G. S. Uhrig, *The European Physical Journal B* **88**, 3 (2015).
- ⁸ E. Manousakis, *Rev. Mod. Phys.* **63**, 1 (1991).
- ⁹ N. Paris, K. Bouadim, F. Hébert, G. G. Batrouni, and R. T. Scalettar, *Phys. Rev. Lett.* **98**, 046403 (2007); K. Bouadim, N. Paris, F. Hébert, G. G. Batrouni, and R. T. Scalettar, *Phys. Rev. B* **76**, 085112 (2007).
- ¹⁰ S. S. Kancharla and E. Dagotto, *Phys. Rev. Lett.* **98**, 016402 (2007).
- ¹¹ A. Garg, H. Krishnamurthy, and M. Randeria, *Phys. Rev. Lett.* **112**, 106406 (2014).
- ¹² F. Wegner, *Annalen der Physik* **506**, 77 (1994).

¹³ H. Krull, N. A. Drescher, and G. S. Uhrig, *Phys. Rev. B* **86**, 125113 (2012).

¹⁴ A. B. Harris and R. V. Lange, *Phys. Rev.* **157**, 295 (1967).

¹⁵ K. A. Chao, J. Spalek, and A. M. Oles, *Journal of Physics C: Solid State Physics* **10**, L271 (1977).

¹⁶ S. A. Hamerla, S. Duffe, and G. S. Uhrig, *Phys. Rev. B* **82**, 235117 (2010).

¹⁷ J. Jędrak and J. Spalek, *Phys. Rev. B* **83**, 104512 (2011).

¹⁸ G. S. Uhrig, K. P. Schmidt, and M. Grüninger, *Phys. Rev. Lett.* **93**, 267003 (2004).

¹⁹ M. Powalski, G. S. Uhrig, and K. P. Schmidt, *Phys. Rev. Lett.* **115**, 207202 (2015).

²⁰ C. Knetter and G. S. Uhrig, *Phys. Rev. Lett.* **92**, 027204 (2004).

²¹ T. Fischer, S. Duffe, and G. S. Uhrig, *New Journal of Physics* **12**, 033048 (2010).

²² C. Knetter and G. Uhrig, *The European Physical Journal B - Condensed Matter and Comp*

²³ S. Kehrein, *The Flow Equation Approach to Many-Particle Systems*, Springer Tracts in Modern Physics, Vol. 217 (Berlin:Springer, 2006).

²⁴ Due to the electron-hole transformation, the 2-QP singlet state is given by $|eh\rangle^{S=0} = (|\uparrow\uparrow\rangle + |\downarrow\downarrow\rangle)/\sqrt{2}$.

²⁵ The value of U_{c2} is slightly lower than the value where Δ_s vanishes in Fig. 4(b) because the off-diagonal terms neglected in the calculation of Δ_s contribute in the MF

- solution favoring Néel ordering.
- ²⁶ H. J. Schulz, Phys. Rev. B **39**, 2940 (1989).
- ²⁷ M. Vojta and O. Rösch, Phys. Rev. B **77**, 094504 (2008).
- ²⁸ M. A. Metlitski and S. Sachdev, Phys. Rev. B **82**, 075128 (2010).
- ²⁹ S. Sachdev and R. La Placa, Phys. Rev. Lett. **111**, 027202 (2013).